INSTITUT DE FRANCE
Académie des sciences

Comptes Rendus

Chimie

Khairul Basyar Baharudin, Nurulhuda Abdullah and Darfizzi Derawi

Synthesis of raspberry-like structure zinc oxide nanoparticles via glycol-solvothermal, low-temperature solvothermal and coprecipitation methods

Volume 24, issue 1 (2021), p. 33-42

Published online: 23 February 2021

https://doi.org/10.5802/crchim.53

Les Comptes Rendus. Chimie *sont membres du*
Centre Mersenne pour l'édition scientifique ouverte
www.centre-mersenne.org
e-ISSN : 1878-1543

Comptes Rendus
Chimie
2021, 24, nº 1, p. 33-42
https://doi.org/10.5802/crchim.53

Full paper / *Article*

Synthesis of raspberry-like structure zinc oxide nanoparticles via glycol-solvothermal, low-temperature solvothermal and coprecipitation methods

Khairul Basyar Baharudin [a, b], Nurulhuda Abdullah [c] and Darfizzi Derawi*, [a]

[a] Laboratory for Biolubricant, Biofuels and Bioenergy Research, Department of Chemical Sciences, Faculty of Science and Technology, Universiti Kebangsaan Malaysia, 43600 UKM Bangi, Selangor, Malaysia

[b] Faculty of Biotechnology and Biomolecular Science, Universiti Putra Malaysia, 43400 UPM Serdang, Selangor, Malaysia

[c] Technology & Engineering Division, Malaysian Rubber Board, 47000, Sungai Buloh, Malaysia

E-mails: basyar@upm.edu.my (K. B. Baharudin), nurulhuda.a@lgm.gov.my (N. Abdullah), darfizzi@ukm.edu.my (D. Derawi)

Abstract. Highly crystalline ZnO nanoparticles with a pure phase and raspberry-like structure were synthesized using three different techniques (glycol-solvothermal, low-temperature solvothermal, and coprecipitation methods). Physisorption analysis and field emission scanning electron microscopy confirmed the large specific surface area of the ZnO nanoparticles with a mesoporous–macroporous structure due to the interstices of aggregated and agglomerated secondary and tertiary ZnO particles. The ZnO nanoparticles from the coprecipitation method presented the best performance among the three products, owing to their highest purity and crystalline phase, large Brunauer–Emmett–Teller surface area (23.0 $m^2 \cdot g^{-1}$) and pore volume, and the finest mesoporous–macroporous structure. ZnO nanoparticles can be used in various applications such as catalysis, biosensing, imaging, drug delivery, and pollution absorption for the purpose of environmental remediation.

Keywords. ZnO, Low-temperature solvothermal, Glycol-solvothermal, Coprecipitation, Nanoparticle.

Manuscript received 25th July 2020, revised 21st October 2020, accepted 22nd October 2020.

1. Introduction

ZnO nanoparticles have been reported to have highly diversified shapes such as flake, raspberry, flower, sheet, wire, and rod morphology, and their dimension can be tuned by synthetic techniques to achieve the best performance in applications [1–3]. In the templated synthesis methods, however, many factors need to be carefully considered to ensure the high crystallinity and purity of ZnO nanoparticles,

* Corresponding author.

for example the stability of the template toward the reaction condition, the pore blockage effect from the wetting behavior of the template, and template removal at the final reaction condition [1].

ZnO nanoparticles in different aspect ratios were successfully prepared using both the solvothermal and coprecipitation methods, by employing different organic solvents as the medium [4–8]. The effects of a given solvent on the particle morphology are well correlated with the dielectric constant of the solvent. A high dielectric constant solvent affects the thermal decomposition of the precursor by increasing the spontaneous ZnO nuclei forms. High polarity of the solvent can also reduce the aspect ratio of the nanomaterial by inhibiting the growth of the ZnO crystal [4,7,8]. Polyols such as ethylene glycol (EG) can act as a reducing agent to form the ZnO nanoparticles [9]. The high dielectric constant and high polarity of liquid polyols allows the effective dissolution of most inorganic compounds and salts [10]. EG can also act as a surface-capping agent and stabilizer that controls the particle morphology and size, by limiting the particle growth and hence preventing the particle agglomeration [11,12].

In this study, raspberry-shaped ZnO nanoparticles with the mesoporous–macroporous structure were prepared by three template-free methods: the glycol-solvothermal method, low-temperature solvothermal method, and coprecipitation method. No other common shape-directing surfactants for ZnO synthesis, such as ethylenediaminetetraacetic acid, sodium dodecyl sulfate, and cetyltrimethylammonium bromide were used [2,13]. Both novel one-pot solvothermal methods in this study involve EG, which acts as a surface-capping agent. It is further elucidated that in the novel low-temperature solvothermal method, the presence of sodium hydroxide (NaOH) as a precipitating agent in the mixed EG:ethanol solvent can reduce the required reaction temperature [14]. Hence, EG can affect the particle morphologies, particle size, the phases, and crystalline purity. Meanwhile, in the two-step coprecipitation method, oxalic acid was used as the precipitation agent for this solution route at low temperature (2–4 °C). The reaction between zinc acetate and oxalic acid took place in a mixed solvent of ethanol and isopropanol to produce an intermediate metal oxalate phase. The intermediate further decomposed during calcination to form the highly crystalline and mesoporous–macroporous structure of raspberry-shaped ZnO nanoparticles.

2. Experimental section

2.1. *Materials*

Analytical grade reagents were used to synthesize the materials in this work without further purification. Zinc acetate dihydrate (99%), ethylene glycol (99.94%), and oxalic acid dihydrate (99%) were purchased from HmbG Chemical, Sigma Aldrich, and Fluka, respectively. Absolute ethanol and 2-propanol were purchased from Fisher Scientific (99.5%). Nickel (II) nitrate hexahydrate (99%) and sodium hydroxide were purchased from Merck.

2.2. *Synthesis of ZnO nanoparticles*

In the glycol-solvothermal modified method, according to the polyol preparation of nanoscale ZnO [12], 0.5 M zinc acetate (ZnAc) was dissolved in 50 mL of EG in a 100 mL beaker by heating at 50 °C with stirring at 300 rpm. Next, the solution was placed in a 50 mL teflon-lined stainless-steel vessel (autoclave), and 1.2 mL deionized water was added. The autoclave was then sealed and heated in a temperature-controlled solvothermal oven (PROTECH, model GOV-100) equipped with a 360° vertical rotator and left rotating at 35 rpm. The autoclave was heated to 180 °C and that temperature was maintained for 3 h. The resulting milky-colored solution was centrifuged and washed three times with ethanol. The as-obtained white precipitates were dried at 70 °C for 18 h in an electric oven, and then ground into a fine powder (denoted as ZnO-S1/EG).

In the one-pot low-temperature solvothermal method, 0.5 M of ZnAc was dissolved in a mixed solvent of 20 mL absolute ethanol and 20 mL EG to form a clear solution. After stirring for about 30 min, the clear solution was transferred into an autoclave. After adding 0.1 g of NaOH, the autoclave was sealed and heated in a temperature-controlled solvothermal oven (PROTECH, model GOV-100) at 80 °C for about 13 h while rotating at 35 rpm. The resulting white ZnO nanoparticles were separated from the cloudy white solution by centrifugation, and washed several times with ethanol to remove unwanted ions and impurities. After drying for about 18 h in an

electric oven at 70 °C, the as-obtained white precipitate was ground into a fine powder and denoted as ZnO-S2/EG.

In the coprecipitation method according to the previous study [15], 0.1 M ZnAc was dissolved in ethanol as solution A. Meanwhile, oxalic acid was dissolved at 0.5 M in a 1.5:1 mixed solvent of 2-propanol:water as solution B. Both solutions were then kept in an ice bath (2–4 °C) for 15 min. Next, solution B was poured slowly into solution A in the ice bath with constant stirring. The result was a uniform and stable milky-white suspension. The suspension was continuously stirred for about 1 h, immersed in an ultrasonic water bath for 15 min, followed by centrifugation. The obtained white precipitate was washed several times with ethanol, and dried for 18 h in an electrical oven at 70 °C. The dried powder was calcined in a muffle furnace at a ramp rate of 5 °C·min^{-1} to 400 °C and that temperature was maintained for 4 h. The product was denoted as ZnO-COP.

2.3. *Characterization of ZnO nanoparticles*

The crystallinity and purity of the obtained materials were characterized using a Shimadzu XRD-6000 powder diffractometer. CuKα (λ = 1.54 Å) radiation was generated at 40 kV and 20 mA from a Philips glass diffraction X-ray tube broad focus 2.7 kW type on each subjected sample at ambient temperature. The continuous scanning rate was set at 2° per second within the 2θ range of 5°–80°. The Scherrer equation was used to calculate the volume-averaged crystallite diameters. A nanoparticle analyzer (Sympatec NANOPHOX, Germany) was used to determine the particles size distribution (PSD). The use of photon cross-correlation spectroscopy (PCCS) technique allows the measurement of particle size in nanometers (nm). Initially, 0.01 g of the ZnO powder was dispersed in 10 mL ethanol in a sample bottle, followed by sonication for 15 min. Then, around 3.5 mL of the well-dispersed solution was put in the acrylic cuvette using a glass dropper for ZnO PSD analysis.

The FTIR spectra were recorded using a Perkin-Elmer 1725X Fourier transform infrared spectrophotometer by the KBr technique. A surface area and pore size analyzer (BELSORP-mini II, BEL, Japan) was used to investigate the surface properties of the materials using nitrogen gas adsorption–desorption technique at 77 K. Each prepared sample was previously degassed at 383 K overnight. The Brunauer–Emmett–Teller (BET) method was used to calculate the specific surface area, while the Barrett–Joyner–Halenda (BJH) method was used to determine the PSD from the nitrogen desorption branches of the isotherm. The particle surface morphology was observed by a field emission scanning electron microscope (FESEM, JEOL model JSM 6700F) operated at the accelerating voltage of 10 kV. The sample was first mounted on an aluminum stub holder using double-sided tape and then coated with an extremely thin layer of platinum using a sputter coater under vacuum to eliminate the possibility of electric charging and thermal loading on the sample during the analysis. The morphology of the ZnO nanoparticles was examined by a transmission electron microscope (TEM, Hitachi model H-7100).

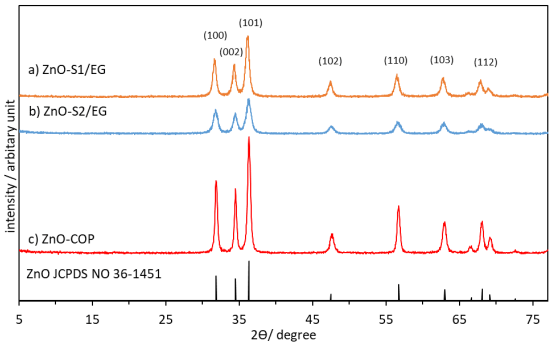

Figure 1. XRD patterns for ZnO nanoparticles synthesized by glycol-solvothermal (a), low-temperature solvothermal (b), and coprecipitation method (c).

3. Results and discussion

3.1. *ZnO nanoparticles structural analysis*

XRD patterns of the ZnO nanoparticles synthesized by three different methods are shown in Figure 1. The as-synthesized ZnO nanoparticles revealed a high degree of crystallization, with similar diffraction profiles but different peak intensity. Nevertheless, all diffraction patterns completely matched the peaks of ZnO with hexagonal-wurtzite structure (JCPDS card No. 36-1451). No other peaks were observed within the detection limit of X-ray diffraction. So,

ZnO nanoparticles obtained by these three methods were all relatively pure in phase. ZnO-S2/EG produced from the low-temperature solvothermal reaction presents broader and less intense ZnO diffraction peaks than those of the other two samples. The broad diffraction lines of ZnO-S2/EG also indicate a smaller volume-averaged crystallite size (13.9 ± 1.0 nm, calculated using the Scherrer equation based on the diffraction pattern at $2\theta = 31.8°$). On the other hand, both ZnO-S1/EG and ZnO-COP demonstrated bigger crystallite sizes of 16.5 ± 2.6 and 22.7 ± 2.6 nm, respectively. The peak broadening and the crystallite size are related to the temperature used in sample synthesis. Both solvothermal methods produced smaller crystallites compared to those by the coprecipitation method. The solvothermal method leads to a faster reaction and a high nucleation rate in the system, thus producing ZnO nanoparticles with pure solid phase, good crystallinity, and smaller particle size [16,17]. Calcination at a relatively higher temperature (400 °C) produced ZnO nanoparticles with better crystallinity, as proven by the more intense and narrower diffraction peaks compared to those from the solvothermal methods.

In the one-pot low-temperature solvothermal method, the mixed solvent can reduce the particle size in ZnO-S2/EG. The presence of EG will increase the cohesiveness of the mixed solvent EG:ethanol, thereby decreasing the ionic diffusion rate. A sufficient amount of OH^- ions is necessary to obtain well-grown ZnO nanoparticles, as the OH^- affects the overall reaction by producing larger and more agglomerated ZnO nanoparticles with lower purity [13,18]. In this case, numerous OH^- ions were provided from both NaOH and the mixed solvent. Overall, the conditions used in these experiments improved the reaction by allowing more interaction between the particles and the capping molecule. As a result, high-purity and finely crystallized ZnO nanoparticles could be produced at a low temperature of 80 °C [14,19]. The one-pot reaction system at low temperature can reduce the particle size, since there are fewer chances for the ZnO clusters to collide and coalesce with each other.

During the synthesis of ZnO-S1/EG (see Figure 2), the acetate anion (CH_3CHOO^-) will chelate the cation Zn^{2+} to form $Zn(CH_3COO)_{2(aq)}$, which cannot completely dissociate in the solution. The intermediate solid phase, $Zn(OH)(CH_3COO)$, had been observed when hydrolysis took place with the addition of water (1) [9,20].

$$Zn(CH_3COO)_2 + H_2O \rightarrow Zn(OH)(CH_3COO) + CH_3COOH \quad (1)$$

During the heating process, the condensation reaction leads to progressive dissolution of $Zn(OH)(CH_3COO)$. At 180 °C (close to the boiling point of the glycol solution), water will act as a reducing agent to form zinc metal which produces Zn–O–Zn bonds, leaving behind either CH_3COOH (2) or H_2O (3) [9].

$$Zn(CH_3COO)_2 + Zn(OH)(CH_3COO) \rightarrow Zn_2(O)(CH_3COO)_2 + CH_3COOH \quad (2)$$

$$Zn(OH)(CH_3COO) + Zn(OH)(CH_3COO) \rightarrow Zn_2(O)(CH_3COO)_2 + H_2O \quad (3)$$

A cation of an electropositive metal, such as Zn^{2+}, cannot be reduced because of the mild reducing power of the glycol solution. In all the glycol-solvothermal reactions discussed above, ZnO was nucleated. When the nucleation process was complete, the addition of intermediate species $Zn(OH)(CH_3COO)$ caused the particles to grow [5,9,20].

In the low-temperature solvothermal method, the reaction of the mixed solution in the autoclave will form $Zn(OH)_2$ precipitate and $Zn(OH)_4^{2-}$. A supersaturated solution of the latter is needed for the crystallization process. The temperature and pressure in the autoclave produced the principal species of Zn^{2+} and OH^- from the unstable $Zn(OH)_2$ precipitate. When $[Zn^{2+}]$ and $[OH^-]$ reached supersaturation, the nucleation process and then the crystal growth of ZnO nanoparticles would occur according to (4) and (5) [16,21]:

$$Zn^{2+} + 4OH^- \rightarrow Zn(OH)_4^{2-} \quad (4)$$

$$Zn(OH)_4^{2-} \rightarrow ZnO + 2(H_2O) + O_2 \quad (5)$$

The decomposition of zinc oxalate dihydrate precursor (α-$ZnC_2O_4{\cdot}2H_2O$) was facilitated by calcination at 400 °C to successfully produce ZnO with a relatively pure phase and good crystallization (6), as indicated by the absence of decomposition above 400 °C in the thermogravimetric-differential thermal gravimetry (TG-DTG) analysis thermogram (Figure 3). The calcination temperature is the main factor to be considered, as it will determine the physicochemical properties of the ZnO nanoparticles: a higher temperature induces compact agglomerates

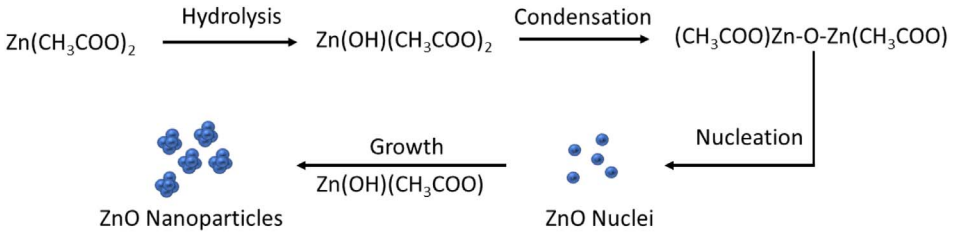

Figure 2. Synthesis of ZnO-S1/EG.

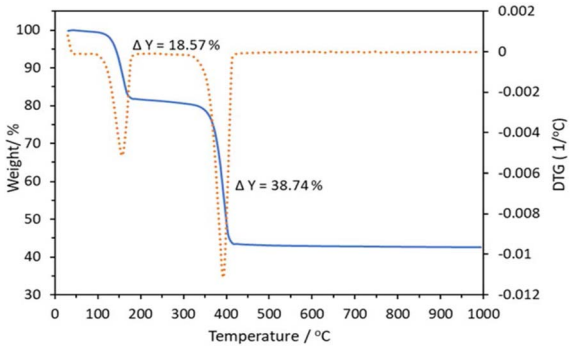

Figure 3. TGA–DTG thermogram of the zinc oxalate dihydrate precursor.

with larger particle size and certainly a smaller surface area [22]. The ice bath (2–4 °C) in the coprecipitation reaction is meant to minimize the loss of cations during centrifugation, as the low temperature will decrease the solubility of metal oxalate. The low dipole moment of 2-propanol is expected to lower the solubility of oxalate, and thus preserve the initial stoichiometry for a more effective coprecipitation reaction between the nearly saturated solutions of acetate and 2-propanol solution of oxalic acid [23,24].

$$\alpha\text{-}ZnC_2O_4 \cdot 2H_2O \rightarrow ZnO + 2H_2O + CO + CO_2 \quad (6)$$

3.2. *Functional group analysis*

The FTIR spectra revealed a series of absorption peaks in the region of 300–2500 cm^{-1}, which verified the ZnO nanoparticle formation and also indicated the presence of various functional groups on the ZnO samples (Figure 4). The formation of highly pure ZnO nanoparticles was verified by the ZnO peak at around 300–400 cm^{-1} [2]. The presence of broad band at around 500–1200 cm^{-1} is due to the metal-oxygen

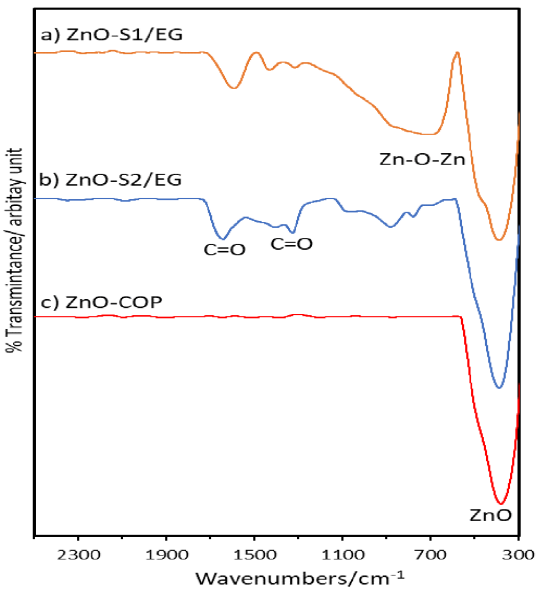

Figure 4. FTIR spectra for ZnO nanoparticles synthesized by glycol-solvothermal (a), low-temperature solvothermal (b) and coprecipitation method (c).

lattice vibrations (Zn–O–Zn) in this region due to the presence of water molecules in the synthesis process [12,23]. The weak bands at around 1640 and 1330 cm^{-1} correspond to the carboxylate species liberated from the starting material, namely either acetate or EG after decomposition and reaction in the solvothermal process [14,25,26]. ZnO-COP emerge to be the highest purity among the three mentioned methods approved by the FTIR spectra analysis at Figure 4.

3.3. *Particles morphology*

ZnO nanoparticles could form different nanostructures, as the small building units arrange and

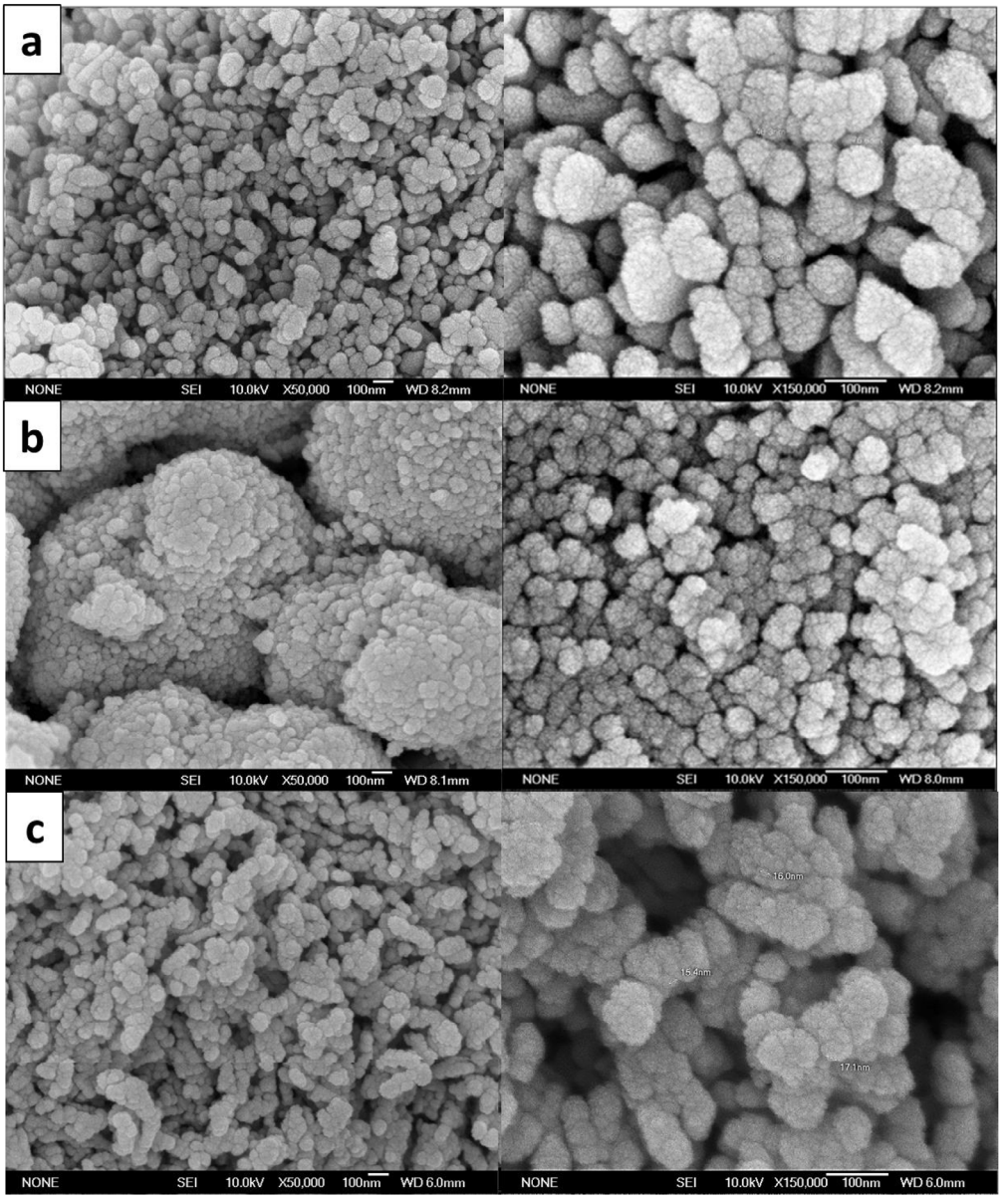

Figure 5. FESEM micrographs for ZnO nanoparticles synthesized by glycol-solvothermal (a) low-temperature solvothermal, (b) and coprecipitation method, and (c) at 50 K (left) and 150 K (right) magnification.

agglomerate in various configurations [27]. Aggregated and compact particles with a raspberry-like shape were seen in all three samples (Figure 5). These uniform, large, and monodispersed structures were comprised of extremely small primary particles aggregating at random orientations to form secondary or even tertiary particles. The adherence between primary particles is due to weak non-covalent interactions (van der Waals forces, Coulomb interaction, and hydrogen bonds) [13,15]. The use of different reaction media (EG:water and EG:ethanol) in the synthesis protocols is a key in controlling the nucleation, crystal growth orientation, and consequently the size of the raspberry-like ZnO nanostructure [4,19,28].

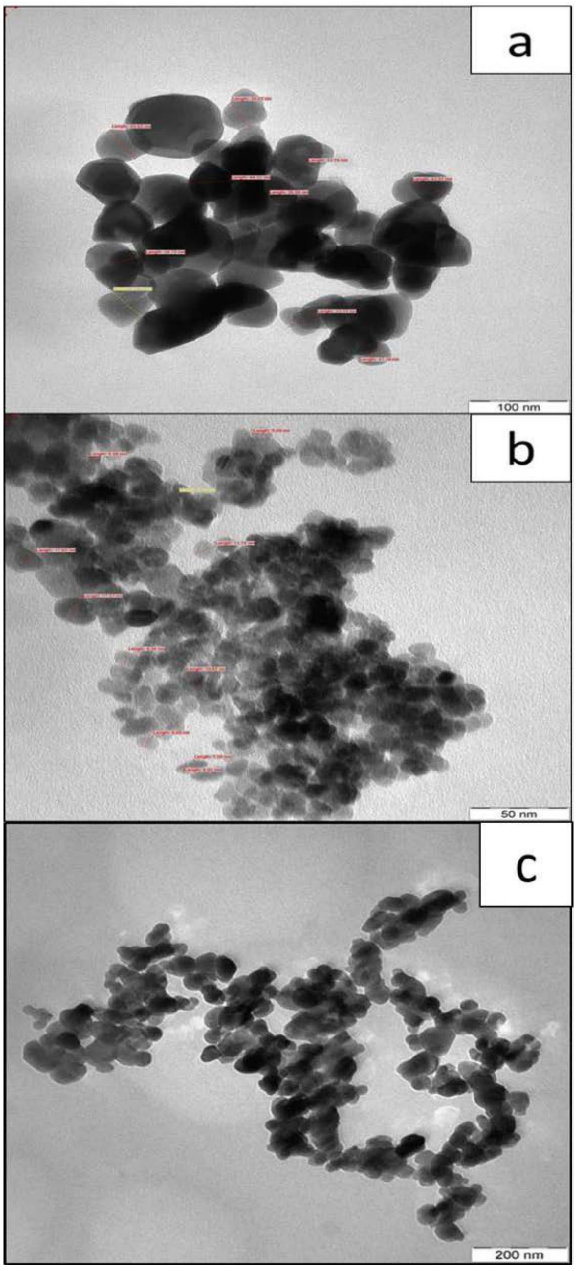

Figure 6. TEM images for ZnO nanoparticles synthesized by (a) glycol-solvothermal, (b) low-temperature solvothermal, and (c) coprecipitation method (c).

In both solvothermal methods, the physicochemical and molecular structure of EG have the utmost influence on the raspberry-like structure produced from controllable agglomeration of ZnO nanoparticles. This is due to the shape-directing and surface-capping capacity of EG. The non-polar EG molecules with a hydroxyl group at the end could effectively attach and adsorb onto the polar surface of ZnO nanoparticles. Such adsorption will further restrict the growth of ZnO along the [0001] directions, ensuring that the primary particles retain their morphology and size. The Zn^{2+} ions that provide the polar (0001) plane of ZnO will form coordination complexes of glycol-Zn^{2+} on the same plane [14, 29,30]. The surface energy of the [0001] plane will be lowered by the capping of glycol, resulting in a decreased growth rate along this plane. Then, the raspberry-like structure of the secondary or even tertiary particles is formed. Thus, the bonding of Zn^{2+}–EG–Zn^{2+} between primary ZnO particles and the formation of secondary/tertiary particles are explained. Meanwhile, 2-propanol plays a crucial role in controlling the nucleation and crystal orientation in the coprecipitation method, as the subsequent decomposition of as-obtained zinc oxalate dihydrate precursor will also form small ZnO particles [15,28,31]. In addition, further analysis revealed the effect of the aggregation of isotropic particles on the final shape of the formed ZnO-COP particles. Dispersive forces and electrostatic interparticle attraction are the main factors controlling aggregation. Isotropic aggregation typically leads to the formation of raspberry-like particles. Such aggregation occurs in the isoelectric point region.

Notably, TEM analysis also supported the result shown in Figure 6. Agglomeration in the form of aggregated, compact raspberry structures were further verified by the TEM results. The existence of large particles in TEM images was related to the aggregation of small or primary particles, affording large compact secondary or even tertiary agglomerated particles as illustrated by Figure 7 and verified by FESEM analysis (Figure 5).

3.4. *Particles size distribution*

Figure 8 reveals that a unimodal and narrow PSD was successfully obtained by three different synthetic methods. In the PCCS technique, the measurement is based on the distribution of primary particles and to some extent the secondary or possibly tertiary particles. ZnO-S2/EG gives a narrower unimodal

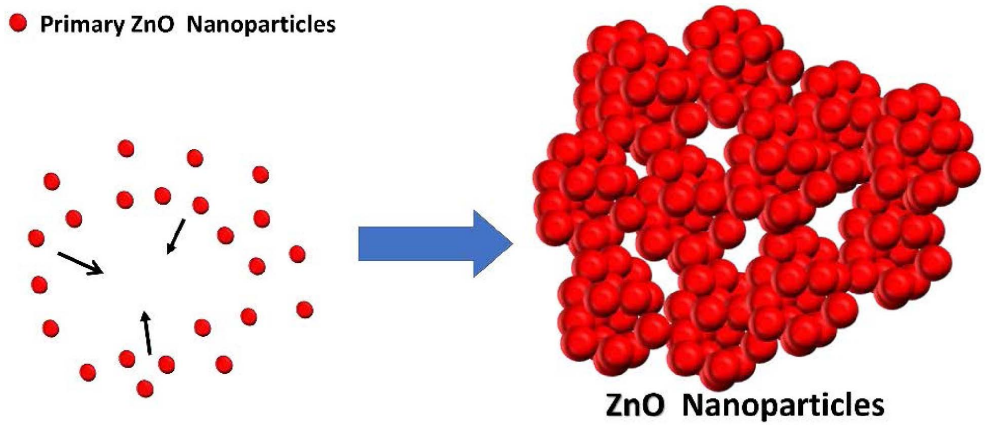

Figure 7. Aggregation of primary ZnO particles in forming raspberry-like structure.

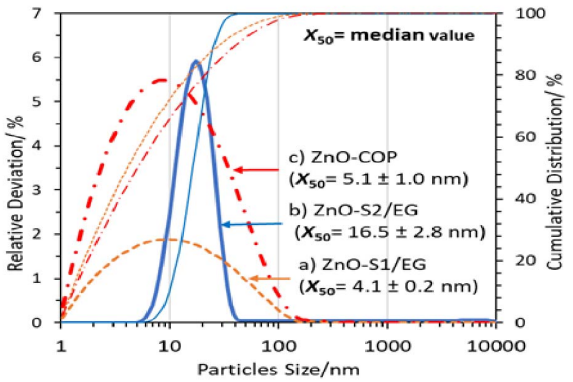

Figure 8. PSD of ZnO nanoparticles synthesized by glycol-solvothermal (a), low-temperature solvothermal (b) and coprecipitation method (c).

PSD compared to ZnO-S1/EG and ZnO-COP, indicating that more uniform particle shape and size can be achieved by the low-temperature solvothermal method. On the other hand, the broader PSDs of ZnO-S1/EG and ZnO-COP give a smaller average particle size (x_{50}) compared to ZnO-S2/EG. Hence, a higher reaction temperature will lead to less uniform ZnO nanoparticles that create a broader PSD.

The PSD results further proved the presence of primary ZnO particles that aggregate to form secondary/tertiary particles, in accordance to the FE-SEM micrographs discussed above. However, there is a poor correlation between the measured PSD and the crystallite size calculated from Scherrer equation. x_{50} being less than the crystallite size for ZnO-S1/EG and ZnO-COP is related to the aggregation and agglomeration of primary particles. The self-assembled crystallites have preferentially aligned crystal planes, while the X-ray used in diffraction analysis is broad and could only "see" them as single crystals. The sonication of ZnO nanoparticles in ethanol prior to the PCSS analysis of PSD could disperse the aggregated particles, thus contributing to the smaller measured particle size. Hence, the XRD technique could give larger crystallite sizes [13].

3.5. *Surface area analysis*

The ZnO nanoparticles synthesized using the low-temperature solvothermal method demonstrate a high BET specific surface area of 40.4 $m^2 \cdot g^{-1}$, compared with 12.8 and 23.0 $m^2 \cdot g^{-1}$ for the glycol-solvothermal and coprecipitation methods, respectively. Generally, a larger specific surface area is preferable because it will increase the surface density and enhance the intermolecular surface interactions. The nitrogen adsorption–desorption isotherms (Figure 9) can be classified as Type IV with H_3 hysteresis loop, which indicates a mesoporous–macroporous type of material [32]. The presence of interparticle pores between the secondary and tertiary ZnO nanoparticles is due to the particle agglomeration and aggregation. Hence, the normally nonporous structure of ZnO now appears as a mesoporous–macroporous material, as demonstrated previously by FESEM micrographs [33]. ZnO-COP shows the

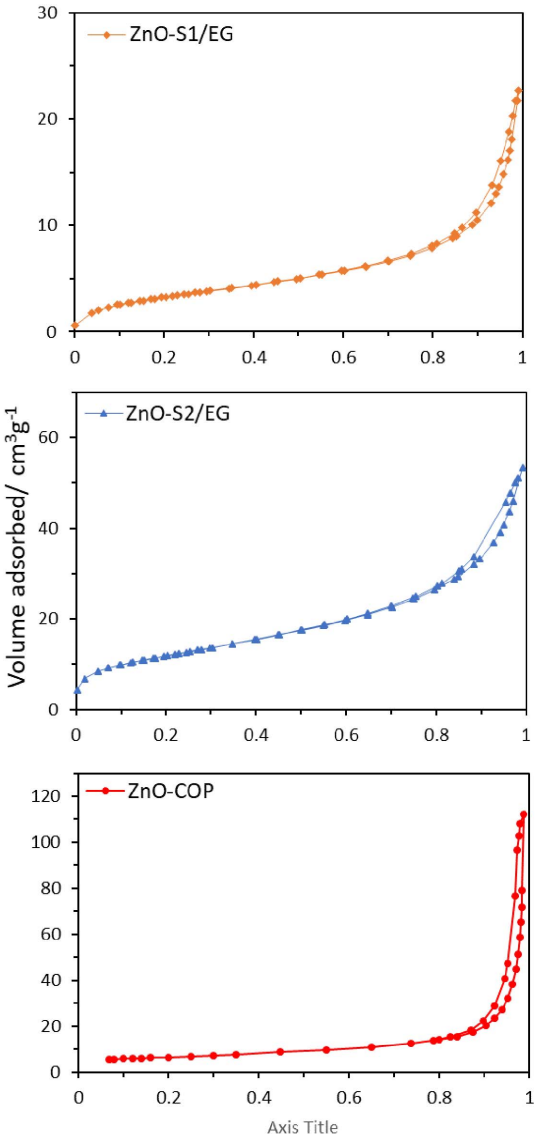

Figure 9. Nitrogen adsorption–desorption isotherms of ZnO synthesized glycol-solvothermal (a), low-temperature solvothermal (b) and coprecipitation method (c).

adsorption pattern of an adsorbent, reaching a maximum uptake capacity of ~120 $cm^3 \cdot g^{-1}$ at standard temperature pressure, while those for ZnO-S1/EG and ZnO-S2/EG are significantly lower (~25 and ~50 $cm^3 \cdot g^{-1}$, respectively). The latter's low uptake of nitrogen reflects the lower pore volume of these ZnO nanoparticles.

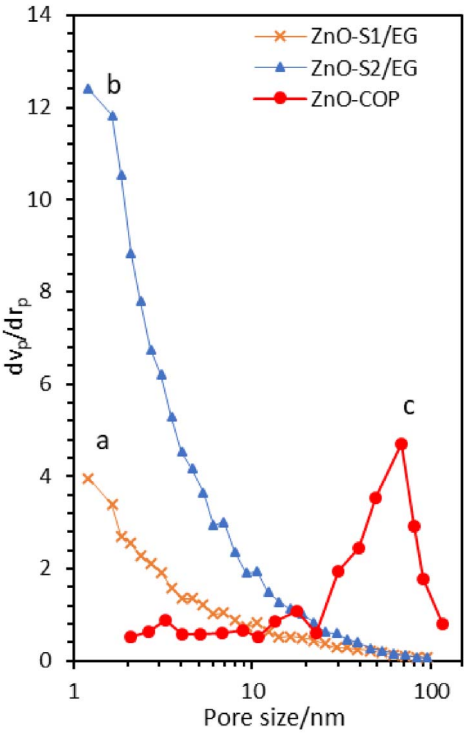

Figure 10. BJH pore size distribution of ZnO synthesized glycol-solvothermal (a), low-temperature solvothermal (b) and coprecipitation method (c).

Figure 10 depicts the pore size distribution of ZnO nanoparticles obtained from BJH desorption. The ZnO-S1/EG and ZnO-S2/EG samples show almost identical profiles, with a broad pore size distribution within 1–100 nm and a declining trend versus pore size. These peaks correspond to interparticle pores within the raspberry-like secondary particles. In contrast, ZnO-COP clearly shows a trimodal broad pore size distribution. The first low-intensity peak appears at around 2–3 nm, and the second broad distribution occurs at around 15–20 nm. Both are mesopores that correspond to the interparticle voids formed by the agglomeration of small primary ZnO particles. Finally, there is a third broad distribution at around 30–100 nm with a maximum at around 50–70 nm. This mesoporous–macroporous range formation peak corresponds to the large pores between the secondary or tertiary particles. The presence of a mesoporous–macroporous structure is not expected from ZnO. However, BJH analysis coupled with N_2

adsorption–desorption isotherms proved that these interparticle pores were indeed formed by the agglomeration and aggregation of small ZnO primary particles into secondary and tertiary particles.

4. Conclusions

Raspberry-like ZnO nanoparticles with good crystallinity and mesoporous–macroporous structure were successfully synthesized using three different techniques, namely glycol-solvothermal, low-temperature solvothermal, and coprecipitation methods, by employing different organic solvents as the medium. The mesoporous–macroporous structure of ZnO nanoparticles with high surface area and pore volume is potentially to be applied for surface-based science applications such as catalysis, biosensing, imaging, drug delivery as well as pollution absorption for the purpose of environmental remediation.

Acknowledgments

The authors are grateful for financial support through the Newton-Ungku Omar Fund, NA150407 provided by the Royal Society, UK (60888) and the Academy of Science Malaysia/MIGHT (ST-2016–006). This work was additionally supported by the Universiti Kebangsaan Malaysia through the grant no. DIP-2020-007 and the Ministry of Higher Education (FRGS/1/2020/STG04/UKM/02/1). We gratefully acknowledge the research facilities provided by Aston University, Universiti Kebangsaan Malaysia, and Universiti Putra Malaysia. We would also like to thank the Ministry of Education for the PhD scholarship provided to Hadiah Latihan Persekutuan. The authors appreciate all the services and contributions given by the frontliners during the difficult period facing the threat of COVID-19.

References

[1] M. Z. Hussein, W. H. W. N. Azmin, M. Mustafa, A. H. Yahaya, *J. Inorg. Biochem.*, 2009, **103**, 1145-1150.
[2] D. Ramimoghadam, M. Z. Bin Hussein, Y. H. Taufiq-Yap, *Int. J. Mol. Sci.*, 2012, **13**, 13275-13293.
[3] K. Mohan, B. Kumar, E. Appala, M. Sinha, K. Siva, P. Sreedhara, *Spectrochim. Acta A*, 2013, **104**, 171-174.
[4] K. G. Kanade, B. B. Kale, R. C. Aiyer, B. K. Das, *Mater. Res. Bull.*, 2006, **41**, 590-600.
[5] J. Wojnarowicz, A. Opalinska, T. Chudoba, S. Gierlotka, R. Mukhovskyi, E. Pietrzykowska, K. Sobczak, W. Lojkowski, *J. Nanomater.*, 2016, **2016**, article no. 2789871.
[6] S. K. N. Ayudhya, P. Tonto, O. Mekasuwandumrong, V. Pavarajarn, P. Praserthdam, *Cryst. Growth Des.*, 2006, **6**, 2446-2450.
[7] A. Šarić, I. Despotović, G. Štefanić, *J. Mol. Struct.*, 2019, **1178**, 251-260.
[8] A. Ali, S. Ambreen, R. Javed, S. Tabassum, I. ul Haq, M. Zia, *Mater. Sci. Eng. C*, 2017, **74**, 137-145.
[9] L. Poul, S. Ammar, N. Jouini, F. Fievet, F. Villain, *J. Sol-Gel Sci. Technol.*, 2003, **26**, 261-265.
[10] C. Feldmann, *Solid State Sci.*, 2005, **7**, 868-873.
[11] A. Mezni, F. Kouki, S. Romdhane, B. Warot-Fonrose, S. Jouli, A. Mlayah, L. Samia Smiri, *Mater. Lett.*, 2012, **86**, 153-156.
[12] B. W. Chieng, Y. Y. Loo, *Mater. Lett.*, 2012, **73**, 78-82.
[13] S. Bernik, A. Rečnik, M. Šćepanović, Z. Branković, M. Počuča Nešić, K. Vojisavljević, D. Luković Golić, G. Branković, N. Daneu, D. Poleti, *Nanotechnology*, 2011, **22**, article no. 395603.
[14] A. Dakhlaoui, M. Jendoubi, L. S. Smiri, A. Kanaev, N. Jouini, *J. Cryst. Growth*, 2009, **311**, 3989-3996.
[15] K. B. Baharudin, N. Abdullah, D. Derawi, *Mater. Res. Express*, 2018, **5**, article no. 125018.
[16] H. Y. Xu, H. Wang, Y. C. Zhang, W. L. He, M. K. Zhu, B. Wang, H. Yan, *Ceram. Int.*, 2004, **30**, 93-97.
[17] T. Ghoshal, S. Biswas, M. Paul, S. K. De, *J. Nanosci. Nanotechnol.*, 2009, **9**, 5973-5980.
[18] K. Harun, F. Hussain, A. Purwanto, B. Sahraoui, A. Zawadzka, A. A. Mohamad, *Mater. Res. Express*, 2017, **4**, article no. 085908.
[19] P. B. Khoza, M. J. Moloto, L. M. Sikhwivhilu, *J. Nanotechnol.*, 2012, **2012**, article no. 195106.
[20] S. Lee, S. Jeong, D. Kim, S. Hwang, M. Jeon, J. Moon, *Superlattices Microstruct.*, 2008, **43**, 330-339.
[21] T. Ghoshal, S. Kar, J. Ghatak, S. Chaudhuri, *Mater. Res. Bull.*, 2008, **43**, 2228-2238.
[22] M. Shohel, M. S. Miran, M. A. B. H. Susan, M. Y. A. Mollah, *Res. Chem. Intermed.*, 2016, **42**, 5281-5297.
[23] K. G. Kanade, B. B. Kale, R. C. Aiyer, B. K. Das, *Mater. Res. Bull.*, 2006, **41**, 590-600.
[24] G. E. Shter, G. S. Grader, *J. Am. Ceram. Soc.*, 1993, **77**, 1436-1440.
[25] N. R. Yogamalar, R. Srinivasan, A. C. Bose, *Opt. Mater. (Amst)*, 2009, **31**, 1570-1574.
[26] D. Krishnan, T. Pradeep, *J. Cryst. Growth*, 2009, **311**, 3889-3897.
[27] A. Eftekhari, F. Molaei, H. Arami, *Mater. Sci. Eng. A*, 2006, **437**, 446-450.
[28] M. Rezapour, N. Talebian, *Mater. Chem. Phys.*, 2011, **129**, 249-255.
[29] L. Zhang, Y. J. Zhu, *Appl. Phys. A*, 2009, **97**, 847-852.
[30] S. K. N. Ayudhya, P. Tonto, O. Mekasuwandumrong, V. Pavarajaran, P. Praserthdam, *Cryst. Growth Des.*, 2006, **6**, 2446-2450.
[31] J. Šubrt, V. Štengl, S. Bakardjieva, L. Szatmary, *Powder Technol.*, 2006, **169**, 33-40.
[32] S. M. Morris, P. F. Fulvio, M. Jaroniec, *J. Am. Chem. Soc.*, 2008, **130**, 15210-15216.
[33] S. A. M. Zobir, Z. Zainal, M. Z. Hussein, *Mater. Chem. Phys.*, 2010, **124**, 477-481.